This is an Accepted Manuscript of an article published by Taylor & Francis in MOLECULAR SIMULATION on 29/07/2015, available online: http://www.tandfonline.com/10.1080/08927022.2015.1059938

Accepted 04 June 2015, available online 29 July 2015.

New insights into the molecular mechanism of methanol-induced inactivation of *Thermomyces lanuginosus* lipase: A molecular dynamics simulation study

Xiaoxue Tong [1], Peter Kamp Busk [1], Lene Lange [1] and Jiayun Pang [2*]

[1] *Section for Sustainable Biotechnology, Department of Chemistry and Bioscience, Aalborg University Copenhagen, Denmark*

[2] *Department of Pharmaceutical, Chemical and Environmental Sciences, Faculty of Engineering and Science, University of Greenwich, Central Avenue, Chatham Maritime, Chatham, Kent ME4 4TB, United Kingdom*

*Corresponding author:

Jiayun Pang, work address: Department of Pharmaceutical, Chemical and Environmental Sciences, Faculty of Engineering and Science, University of Greenwich, Medway Campus, Central Avenue, Chatham Maritime, Kent ME4 4TB, United Kingdom. Telephone +44 (0)208331 9829. E-mail j.pang@gre.ac.uk

Abstract

Methanol intolerance of lipase is a major limitation in lipase-catalyzed methanolysis reactions. In this study, to understand the molecular mechanism of methanol-induced inactivation of lipases, we performed molecular dynamics (MD) simulations of *Thermomyces lanuginosus* lipase (TLL) in water and methanol and compared the observed structural and dynamic properties. The solvent accessibility analysis showed that in methanol, polar residues tended to be buried away from the solvent while non-polar residues tended to be more solvent-exposed in comparison to those in water. Moreover, we observed that in methanol, the van der Waals packing of the core residues in two hydrophobic regions of TLL became weak. Additionally, the catalytically relevant hydrogen bond between Asp^{201} OD2 and His^{258} ND1 in the active site was broken when the enzyme was solvated in methanol. This may affect the stability of the tetrahedral intermediates in the catalytic cycle of TLL. Furthermore, compared to those in water, some enzyme surface residues displayed enhanced movement in methanol with higher Cα root-mean-square atomic positional fluctuation values. One of such methanol-affecting surface residues (Ile^{241}) was chosen for mutation, and MD simulation of the I241E mutant in methanol was conducted. The structural analysis of the mutant showed that replacing a non-polar surface residue with an acidic one at position 241 contributed to the stabilization of enzyme structure in methanol. Ultimately, these results, while providing molecular-level insights into the destabilizing effect of methanol on TLL, highlight the importance of surface residue redesign to improve the stability of lipases in methanol environments.

Keywords

Thermomyces lanuginosus lipase; methanol intolerance; molecular dynamics simulation; rational design; protein stability

Abbreviations TLL: *Thermomyces lanuginosus* lipase; CALB: *Candida antarctica* lipase B; MD: Molecular dynamics; WT: Wild type; DMSO: Dimethyl sulfoxide; Cα RMSF: Cα root-mean-square atomic positional fluctuation; SASA: Solvent accessible surface area; RMSD: Root-mean-square deviation; Rg: Radius of gyration

1 Introduction

Biodiesel, an alternative to diesel fuel, is produced by transforming oil into fatty acid alkyl esters in the presence of alcohols, such as methanol or ethanol, via chemical catalysts or biocatalysts. Enzymatic biodiesel production with lipases has attracted broad attention from both academia and industry since it offers an environmentally friendly condition with simplified separation and purification processes compared to the chemical production of biodiesel [1], [2], [3] and [4]. Recently, lipase from ascomycetous fungus *Thermomyces lanuginosus* (TLL) has been explored for enzymatic biodiesel production due to its high methanolysis activity [5], [6], [7] and [8]. In TLL-catalyzed methanolysis reaction between crude non-degummed soybean oil and methanol, the yield of fatty acid methyl ester (biodiesel) was over 96% (w/w of oil) in the presence of 3-5% (w/w of oil) water [4]. This indicates that TLL is an efficient, convenient and soluble biocatalyst for cost-effective biodiesel production in water-requiring systems [4], [6] and [8]. Despite its great promise, the use of TLL to catalyze methanolysis reactions has its limitation because the presence of high concentrations of methanol can inactivate the enzyme [4], [5] and [8]. In this context, understanding the molecular basis of methanol-induced inactivation of TLL, and applying this knowledge to rationally engineer TLL, e.g., fine tuning the enzyme structure, to improve its methanol tolerance will facilitate TLL's application as a suitable industrial biocatalyst for biodiesel production.

The mature TLL consists of 269 amino acids forming a single chain protein (excluding the signal and propeptide sequences). Several crystal structures of TLL have been solved. They display a typical α/β hydrolase fold [9] and [10], stabilized by three disulfide bonds (Cys^{22}-Cys^{268}, Cys^{41}- Cys^{36} and Cys^{104}-Cys^{107}) [8]. Similar to other lipases, TLL has a helical lid, which is composed of residues 86-92, and two hinge regions of the lid, which consists of residues 82-85 and 93-96 [8]. The lid, in its so-called closed conformation, shields the active site in aqueous solution. Upon ligand binding, the lid undergoes a conformational rearrangement, which makes the active site accessible to the lipid substrate by a hinge bending movement resulting in the exposure of a large hydrophobic protein-lipid interaction

surface [8] and [11]. The essential functional center of TLL is the catalytic triad Ser^{146}-His^{258}-Asp^{201}. Another important component of the active center of TLL is the so-called oxyanion hole, formed by the backbone NH groups of Ser^{83} and Leu^{147}. The catalytic mechanism of TLL-catalyzed methanolysis reaction between methanol and ester molecules or hydrolysis reaction between water and ester molecules is illustrated in Fig. 1. In the acylation step, the deprotonated Ser^{146} hydroxyl group nucleophilically attacks the carbonyl carbon of ester substrate generating the first tetrahedral intermediate stabilized by the oxyanion hole. The first product, an alcohol molecule leaves the active site and an acyl enzyme intermediate is formed. In the subsequent deacylation step, either a methanol molecule (methanolysis) or a water molecule (hydrolysis) enters the active site and performs the second nucleophilic attack on the carbonyl carbon of the acyl enzyme forming the second tetrahedral intermediate. Upon reformation of the carbonyl, a transacylation product is released and Ser^{146} becomes free for the next catalytic cycle [12].

Previous experimental studies have examined the effect of alcohol on the structure and function of lipases in aqueous alcoholic solutions. On one hand, it was reported that the active site was perturbed structurally by the presence of alcohols. A nuclear magnetic resonance (NMR) study of *Bacillus subtilis* lipase in 40% (v/v) methanol and 30% (v/v) isopropanol showed that alcohol molecules caused significant perturbations of the chemical shifts of residues in the active site or its close vicinity, suggesting that alcohol-induced inactivation of the enzyme was directly linked to the conformational change in the active site [13]. In addition, Mattos and co-workers solved the crystal structures of porcine pancreatic elastase (serine protease that belongs to the α/β-hydrolase fold family with the Ser^{206}-His^{60}-Asp^{108} triad) in 80% (v/v) isopropanol, 80% (v/v) ethanol and 40% (v/v) trifluoroethanol, respectively [14]. They found that alcohol molecules clustered in the enzyme active site, changing the side-chain conformations of active site residues. On the other hand, Tanaka *et al*. observed that the rate of thermal unfolding of *Pseudomonas cepacia* lipase was accelerated in the presence of longer hydrophobic alkyl chain of alcohols (methanol, ethanol, propanol and butanol) as measured by adiabatic scanning calorimetry [15]. The effect of alcohols on the thermal

unfolding of enzyme is interpreted as that increased hydrophobicity of alcohol solvent weakens the intra-molecular hydrophobic interaction between the protein's side chains and thus destabilize its tertiary structure. Although these experimental studies support the notion of a destabilizing effect of alcohol on lipase, more direct mechanistic details, in particular how alcohol affects the enzymatic reaction mechanism are still needed.

In recent years, molecular dynamics (MD) simulations have emerged as a useful complement to the experimental studies for understanding the underlying molecular mechanism of methanol-induced inactivation of lipases. Li *et al.* reported that methanol molecules could reach into the active site and interacted with catalytic triad residues of *Candida antarctica* lipase B (CALB) [16]. The interaction destroyed the hydrogen bond (H-bond) between Ser^{105} OG (Ser^{105} hydroxyl oxygen atom) and His^{224} NE2 (nitrogen atom from His^{224} ring), as indicated by the distance of Ser^{105} OG-His^{224} NE2 being longer than 3.5 Å. Park *et al.* observed that some CALB surface residues displayed enhanced movement with higher root-mean-square deviations (RMSDs) in methanol than in water [17]. Substituting these methanol-affecting surface residues by site-directed mutagenesis to lower their RMSDs improved the enzyme stability in 80% (v/v) methanol. Li *et al.* found that the native hydrophobic interactions in *Yarrowia lipolytica* lipase were weakened at high methanol concentrations (more than 30%), which disrupted the tertiary structure of the enzyme [18]. These MD simulation studies highlight several underlying structural and dynamical changes in lipases induced by the presence of methanol molecules, i.e., disrupting the catalytically relevant H-bond in the active site, inducing enhanced movement of some enzyme surface residues and weakening the intra-protein hydrophobic interactions.

In the present study, we used a computational approach to understand the molecular mechanism of methanol-induced inactivation of TLL. MD simulations of wild type (WT) TLL in water and methanol were performed for 5 ns. Changes in both the overall structure and the active site conformation of the enzyme induced by methanol were observed. In particular, some surface residues exhibited enhanced flexibility in methanol. We subsequently mutated one of the methanol-affecting surface residues, Ile^{241} to glutamic acid and ran a 5 ns

MD simulation of the I241E mutant in methanol. The structural analysis of the mutant showed that replacing a non-polar residue with an acidic one at position 241 contributed to the stabilization of enzyme structure in methanol. Our computational studies provide a detailed molecular-level understanding of the destabilizing effect of methanol on TLL, and highlight the utility of combining MD simulation with surface residue redesign to rationally engineer industrially important lipases for improved methanol tolerance.

2 Materials and methods

2.1 Simulation model preparation

The X-ray crystal structure of TLL was taken from Protein Data Bank (PDB) (PDB ID: 1EIN) [8]. It is an open conformation of TLL with a phospho-lipid (diundecyl phosphatidyl choline, PLC) present in the active site. The 3D structure of the I241E mutant was predicted via RosettaDesign based on the WT TLL structure with isoleucine 241 replaced by glutamic acid [19] and [20]. The structure of the ester substrate, i.e. methyl caproate, was constructed using program GaussView 5.0.9 [21] and then superimposed onto PLC. The protonation states of titratable residues were determined at pH 7.0 using H++, a web-based system that computes pK values of ionizable groups in enzymes [22]. All crystallographic water and PLC molecules were removed and hydrogen atoms were added using the Leap program within AMBER12 program package [23] and [24].

The system comprising 269 amino acid residues and ester substrate was solvated in a rectangular solvent box with at least 8 Å between the edge of the box and protein. TIP3PBOX model and MEOHBOX model were used for water and methanol solvation environment, respectively [25] and [26]. Sodium ions were added to neutralize overall charge of the system. The protein was modelled using Amber ff99SB force field while the ester substrate was represented by the general Amber force field (GAFF) [27] and [28].

2.2 MD Simulations

Initially, the solvated system was energy minimized by a two-stage approach. In the first stage, solvent and ions were minimized with 500 steps of the steepest descent method followed by 1500 steps of the conjugate gradient method while both the enzyme and the substrate were fixed. In the second stage, the entire system was minimized with 200 steps of the steepest descent method followed by 3800 steps of the conjugate gradient method. Following minimization, the system was heated to 298 K within 20 ps under the constant volume periodic boundary condition. The system was then equilibrated for 200 ps under the constant pressure periodic boundary condition with an average pressure of 1 bar. Production simulations were performed at 298 K and 1 bar for 5 ns. To avoid the ester substrate diffusing away from the active site, three pairwise distance restraints (less than 3 Å with the force constant of 50 $kcal.mol^{-1}.Å^{-2}$) were incorporated during MD simulations, i.e., distance between OG from Ser^{146} and C1 from the ester substrate, distance between O1 from the ester substrate and H from Leu^{147} and distance between O1 from the ester substrate and H from Ser^{83} (Fig. 1) [29]. The long-range electrostatic interactions were treated using particle mesh Ewald method with cut-off distance at 8 Å. SHAKE algorithm was used to constrain bonds involving hydrogen atoms [30]. Production trajectories were collected at every 250 steps (0.5 ps) with a step size of 2 fs. Cpptraj program within Amber12 was used for processing and analyzing trajectories [31]. Configurations in the trajectories were visualized with VMD software [32].

3 Results and Discussions

3.1 The overall conformational changes induced by methanol

To evaluate the structural stability of TLL in water and methanol, the RMSDs of backbone heavy atoms were calculated, as shown in Fig. 2A. For the WT TLL simulated in water, the RMSDs became stable after 500 ps of simulation, reaching a plateau between 0.9 and 1.3 Å. For the WT TLL simulated in methanol, the RMSDs fluctuated between 0.9 and 1.2 Å after 500 ps and exhibited slightly lower RMSDs compared to the WT in water in most of the

simulation. The radius of gyration (Rg), which represents the maximal distance between any atom and geometry center of the enzyme, can be used to determine the compactness of enzyme structure within MD simulation timescale [33]. The WT TLL solvated in water was characterized by a higher average Rg value (17.4 Å ± 0.1) than the one in methanol (17.2 Å ± 0.1) (Fig. 2B), indicating that TLL expanded slightly in water.

TLL is a globular α/β-type protein containing eight central β-strands that are flanked on both sides by six α-helices [8]. We compared the secondary structure contents of WT TLL in water and methanol (Supplementary Fig. S1). Three regions (residues 23-26, residues 114-119 and residues 241-244) displayed noticeably different secondary structural types in the two solvents (Fig. 3). Furthermore, the last structures from the simulations were superimposed onto the initial crystallographic structure of TLL (Fig. 4). It was observed that in water, residues 114-119 which originally displayed α-helix structure in crystallization medium changed to turn structure, and residues 23-26 changed from 3_{10}-helix to turn (Fig. 4A). In methanol, the secondary structural type of residues 241-244 was transformed from turn to 3_{10}-helix (Fig. 4B), although overall, there is no obvious loss in its secondary structure when TLL is solvated in methanol. The result obtained from MD simulation of WT TLL in methanol is consistent with a previous circular dichroism spectra study of WT TLL in high concentration isopropanol solutions (up to 50%), which revealed that isopropanol molecules did not cause major alterations in secondary structure, although the enzyme became completely inactive in 50% isopropanol [34]. X-ray structures of serine proteases, subtilisin Carlsberg and porcine pancreatic elastase, crystallized in neat acetonitrile, 80% (v/v) isopropanol and 80% (v/v) ethanol, respectively, also confirmed a native-like secondary structure of each enzyme [35] and [14].

Changes in hydrogen-bonding interactions for WT TLL in the two solvents were also investigated. As shown in Fig. 5B, in most of the simulation, the number of intra-protein backbone H-bonds present in WT TLL was marginally higher in methanol (70 ± 5 H-bonds on average) than in water (65 ± 6 H-bonds on average), which could be responsible for the reduced flexibility of backbone structure in methanol as seen in the RMSD analysis (Fig. 2A).

The number of backbone H-bonds present in WT TLL is lower in each solvent as compared to that in the crystal structure (89 H-bonds). Additionally, as seen in Fig. 5A, the population of overall intra-protein H-bonds present in WT TLL was higher in methanol (156 ± 7 H-bonds) than in water (132 ± 8 H-bonds) and in the crystal structure (129 H-bonds). Methanol is a weaker H-bond forming solvent compared to water. As shown in Fig. 5C, the hydrogen-bonding interactions between the enzyme and the solvent molecules were significantly reduced when TLL was solvated in methanol (262 ± 8 H-bonds in methanol versus 402 ± 11 H-bonds in water). Overall, solvation of WT TLL in methanol strengthened the intra-protein hydrogen-bonding interactions.

Furthermore, the solvent accessible surface area (SASA) of WT TLL in two solvents was calculated using the linear combinations of pairwise overlaps algorithm [36], as shown in Fig. 6. Consistent with Rg values, the average SASA of WT TLL in water was 11541.6 $Å^2$ ± 159.1, increased by 6% relative to that in methanol (10871.7 $Å^2$ ± 152.1). The total SASA could be divided into non-polar, polar uncharged and polar charged surface area based on the character of residues' side chains. As shown in Fig. 6, the increased total SASA of WT TLL in water was due to the increased solvent exposure of polar residues, both charged (4124.3 $Å^2$ in water versus 3548.5 $Å^2$ in methanol) and uncharged ones (3406.7 $Å^2$ in water versus 3260.8 $Å^2$ in methanol). In contrast, the solvent exposure of non-polar residues slightly increased in methanol (4062.3 $Å^2$) compared to in water (4010.6 $Å^2$). This indicates that in methanol, polar residues tend to be buried away from the solvent while non-polar residues tend to be more solvent-exposed in comparison to those in water. Moreover, we observed that the van der Waals packing between the core residues (Leu^{52}-Leu^{69}, Leu^{67}-Ile^{76}, Val^{128}-Val^{140} and Val^{230}-Ile^{235}-Val^{2}) in two hydrophobic regions of TLL (R1 and R2) was tighter in water (Fig. 7A) than in methanol (Fig. 7B). The observation of reduced interactions between the side chains of hydrophobic amino acids of TLL induced by methanol is in agreement with previous experimental studies. A combined fluorescence spectroscopy and catalytic activity study of TLL in high concentration isopropanol solutions (more than 15%) demonstrated that the loosening of its tertiary structure due to reduced hydrophobic interactions led to the activity

loss of enzyme [34]. Gekko *et al*. also reported that addition of acetonitrile to water weakened the hydrophobic bonding capacity of non-polar side chains of lysozyme, leading to the destabilization of its tertiary structure by means of densimetric and refractometric methods [37]. Sashi *et al*. found by fluorescence and NMR methods an alcohol-induced intra-protein hydrophobic collapse of cytochrome c, which led on to the unfolding of cytochrome c [38]. In summary, the destabilizing effect of methanol on the overall structure of TLL could be explained by diminished interactions between the side chains of hydrophobic amino acids, concomitant with a reduced solvent exposure of polar residues and an increased solvent exposure of non-polar residues in methanol.

3.2 Changes within the active site of TLL

The catalytic triad of TLL consists of residues Ser^{146}, His^{258} and Asp^{201}, as shown in Fig. 1. In the enzymatic reaction, NE2-deprotonated His^{258} acts as a base to abstract the proton from the hydroxyl side chain of Ser^{146}, enhancing its nucleophilicity as it attacks the carbonyl carbon of ester substrate. The side chain oxygen of Asp^{201}, on the other hand, acts to stabilize the positive charge on His^{258} once NE2 acquires the proton from Ser^{146}. Hence, the H-bonds between Ser^{146} and His^{258} and between Asp^{201} and His^{258} are crucial for the stabilization of two tetrahedral intermediates along the reaction path [10]. During MD simulations of WT TLL in two solvents, the distance of Ser^{146} OG-His^{258} NE2 was maintained at approximately 2.8 Å (Fig. 8A). The distance between Asp^{201} OD1 (oxygen atom from Asp^{201} side chain) and His^{258} ND1 (nitrogen atom from His^{258} ring) was ~3.0 Å in water and ~2.8 Å in methanol (Fig. 8B). However, the distance between Asp^{201} OD2 (oxygen atom from Asp^{201} side chain) and His^{258} ND1 fluctuated at approximately 4.9 Å in methanol, whereas it fluctuated at a significantly lower value of 2.9 Å in water (Fig. 8C). Therefore, in water, both distances of Asp^{201} OD1-His^{258} ND1 and Asp^{201} OD2-His^{258} ND1 were within the hydrogen-bonding distance (Fig. 9A), while in methanol, only Asp^{201} OD1 can form H-bond with His^{258} ND1 (Fig. 9B). This indicates that, with the weakened stabilizing effect from the side chain oxygen of Asp^{201}, two tetrahedral intermediates may be less stable in methanol than in water.

The observation that methanol could perturb the H-bond between catalytic triad residues of WT TLL is consistent with a previous MD simulation study on CALB, in which the H-bond between Ser^{105} OG and His^{224} NE2 was not preserved in methanol, as indicated by the distance of Ser^{105} OG-His^{224} NE2 being longer than 3.5 Å [39]. In addition, it was reported that the H-bond between Asp^{32} OD1 and His^{64} NE2 was not maintained when subtilisin, a serine protease, was solvated in polar solvents (tetrahydrofuran and acetonitrile) (~2.5 Å in water versus ~7 Å in polar solvents) [40]. Overall, the analysis presented here demonstrates that the overall structural change of TLL induced by methanol, e.g., different hydrogen-bonding patterns and solvent accessibility changes, could directly alter the active site conformation, in particular perturbing H-bond between the crucial catalytic triad residues, thus the stability of tetrahedral intermediates, which may slow down or halt the catalytic cycle of TLL.

3.3 Computational prediction of a stabilizing mutation for TLL

The root-mean-square atomic positional fluctuations (RMSFs) of backbone α-carbon (Cα) atoms of all residues were plotted (Fig. 10), alongside the crystallographic Cα B-factors, which reflect the mobility of their counterparts in crystalline state [41]. As shown in Fig. 10, the Cα RMSFs obtained from MD simulations were in reasonable agreement with the Cα B-factors in terms of identifying the rigid and flexible regions of TLL. It is not surprising that the largest Cα RMSF values in both simulations are associated with the lid region of TLL (residues 82-96).

Contrary to our observation that the overall structure of WT TLL was more flexible in water (Fig. 2A), some residues displayed higher Cα RMSF values in methanol than in water (Fig. 10). This included residues 25-29, 42-47, 100-103, 161-163, 240-241 and 248-249 that are all located on the surface of TLL. The average SASA of each residue in two solvents is listed in Table S1 of the supplementary information. It has been reported that motions of surface residues are linked to the stability of lipase in polar solvents (methanol, acetonitrile, DMSO and dimethylformamide) [17], [42] and [43]. It is also known that polar solvents, as dehydrating agents, are able to bind to the surface residues of enzyme (lipase, protease and

other enzymes), perturbing the essential layer of water that provides enzyme with conformational flexibility needed for catalysis and thus decreasing the enzymatic activity [40], [44], [45], [46], [47], [48], and [49]. Therefore, the capacity of lipases to tolerate polar solvents could be improved by introducing more intra-protein interactions on the flexible surface region or reducing the interactions between polar solvent molecules and enzyme surface residues. For example, introduction of additional H-bonds to increase interactions between enzyme surface residues increased the stability of *Geobacillus stearothermophilus* lipase in 60% (v/v) methanol by 66 folds and doubled its methanolysis activity [42]. Reetz *et al.* performed saturation mutagenesis on the flexible surface residues of *B. subtilis* lipase with higher B-factors and obtained several mutants with markedly enhanced tolerance to the polar solvents (acetonitrile, DMSO and dimethylformamide), which was due to an increase of intra-molecular H-bonds and salt bridges on the surface of enzyme [43]. The stability of CALB in 80% (v/v) methanol can also be enhanced 1.8 folds by increasing the hydrogen-bonding interactions between surface side chains of enzyme and water molecules [17]. Thus, our Cα RMSFs analysis on TLL surface residues, coupled with the structural analysis, e.g., solvent accessibility analysis, provide a concrete knowledge base to rationally select mutation sites for enzyme engineering to improve the methanol tolerance of TLL by fine-tuning its structure. With the goal of rationally engineer TLL to enhance its methanol tolerance, we mutated one of the methanol-affecting surface residues, Ile^{241} to glutamic acid. Ile^{241} was chosen for mutation since it displayed a different secondary structural type in methanol compared to those in water and crystalline state (Fig. 3 and Fig. 4). Moreover, Ile^{241} also had a higher Cα RMSF value in methanol than in water (Fig. 10), and the SASA of Ile^{241} in two solvents varied considerably (Supplementary Table S1). These data indicate that methanol molecules disturb the secondary structural type and dynamic behavior of Ile^{241}. The mutation information (I241E) was obtained by RosettaDesign, a program aiming at finding the lowest free energy sequences for target protein structures and being able to predict new sequences of proteins more stable than their WT [19] and [20]. Based on the RosettaDesign prediction, the mutation (I241E) could lead to a reduction in free energy of 2.1 kcal/mol.

We performed MD simulation of the I241E mutant in methanol and compared its structural properties with those of the WT solvated in methanol. The mutant was stable across the 5 ns MD simulation. RMSDs of the mutant fluctuated between 0.8 Å and 1.3 Å after 500 ps and the final values were close to those of the WT (Fig. 2A). Rg of the mutant did not show substantial variations compared to the WT (Fig. 2B). As shown in Fig. 5A, in most of the simulation, the number of overall intra-protein H-bonds present in the mutant (159 ± 7 H-bonds on average) was slightly higher than that in the WT (156 ± 7 H-bonds on average). On the other hand, as shown in Fig. 6, the average SASA of polar residues (both charge and uncharged) of the mutant was 6994.3 $Å^2$, increased by 3% compared to that of the WT (6809.3 $Å^2$). In addition, the average SASA of non-polar residues of the mutant was 4000.2 $Å^2$, decreased by 2% compared to that of the WT (4062.3 $Å^2$). The solvent accessibility analysis indicates that mutation of surface residue Ile^{241} to glutamic acid tends to shift the solvent exposure of both polar and non-polar residues in methanol towards that of the WT in water, i.e. non-polar residues tend to be buried away from the solvent while polar ones tend to be more solvent-exposed. Moreover, as seen in Fig. 7C, in the mutant, the core residues in hydrophobic regions of R1 and R2 were observed to be more compact. Therefore, it is speculated that the I241E mutant may counteract the deleterious effect of methanol on reducing the interactions between side chains of hydrophobic amino acids of TLL. Interestingly, the catalytically relevant H-bond between Asp^{201} OD2 and His^{258} ND1 was maintained when the mutant was solvated in methanol (Fig. 8C and Fig. 9C). Overall, the structural analysis of the mutant indicates that replacing a non-polar surface residue of TLL with an acidic one at position 241 is able to change the enzyme structure in methanol into the one that resembles what's seen of the WT in water, e.g., tighter hydrophobic packing in R1 and R2 regions (Fig. 7) and retention of the active site structure (Fig. 9). Based on the MD simulation results, the I241E mutation contributed to stabilizing the enzyme structure in methanol.

Previous studies have identified several hydrophobic regions on enzyme surface where methanol solvent molecules tended to accumulate. A NMR study of *B. subtilis* lipase in

methanol showed that methanol molecules exhibited binding preference towards the hydrophobic patches on enzyme surface [11]. A static light-scattering study of lysozyme by Liu and co-workers demonstrated that methanol molecules could be absorbed onto the hydrophobic sites on enzyme surface [45]. Several studies reported that replacing hydrophobic surface residues with polar or charged ones could improve the enzyme's resistance to methanol, which was likely the result of the inhibition of hydrophobic interactions with methanol molecules. Dror *et al.* found that the stability of *G. stearothermophilus* lipase in 60% (v/v) methanol could be enhanced by 21 folds after mutating the surface residue alanine to threonine [42]. Similarly, Park *et al*. found that in 80% (v/v) methanol, CALB mutants A8T and A92E showed 1.5-fold and 1.8-fold higher stability, respectively, relative to the WT [17]. Badoei-Dalfard *et al*. also reported that the *Salinivibrio* zinc-metalloprotease mutants A195E and G203D in 40% (v/v) methanol exhibited both increased stability and activity compared to the WT [50]. In the present study, based on MD simulations, single I241E mutation on the surface of TLL is predicted to be able to help stabilize the enzyme structure in methanol. This is consistent with previous experimental examinations, which demonstrated the effectiveness of single point mutations of hydrophobic surface residues to polar ones [42], [17] and [50]. In addition, based on variations in secondary structural types, Cα RMSFs and SASA of TLL in two solvents, we further predict mutation sites of Asn^{25}, Pro^{29}, Pro^{42}, Ala^{47} and Gly^{161}, which could be subsequently explored for enzyme engineering to improve the methanol tolerance of TLL by fine-tuning its structure.

4 Conclusions

MD simulations of TLL in water and methanol were performed to investigate the effect of methanol on the structural and dynamic properties of TLL. The solvent accessibility analysis showed that in methanol, polar residues tended to be buried away from the solvent while non-polar residues tended to be more solvent-exposed in comparison to those in water. Moreover, we observed that in methanol, the van der Waals packing of the core residues in two

hydrophobic regions of TLL (R1 and R2) became weak. Additionally, the catalytically relevant H-bond between Asp^{201} OD2 and His^{258} ND1 in the active site was broken in methanol. This may affect the stability of tetrahedral intermediates in the catalytic cycle of TLL. Furthermore, some enzyme surface residues displayed enhanced movement with higher Cα RMSF values in methanol than in water. One of such methanol-affecting surface residues (Ile^{241}) was chosen for mutation, and MD simulation of the I241E mutant in methanol was conducted. The structural analysis of the mutant indicates that replacing a non-polar surface residue with an acidic one at position 241 could help stabilize the enzyme structure in methanol. Several improved structural features of the mutant include: (i) maintenance of the H-bond between Asp^{201} OD2 and His^{258} ND1; (ii) enhanced interactions between the side chains of hydrophobic amino acids; (iii) improved intra-protein hydrogen-bonding interactions. In summary, the simulation results presented here unravel several factors that could be related to the methanol intolerance of TLL on the molecular level. The beneficial mutation of Ile^{241} to glutamic acid highlights the importance of surface residue redesign to improve the enzyme stability in methanol environments.

5 Acknowledgements

This work was supported by Aalborg University, Faculty of Science and Technology and by the BioValue/SPIR grant DSF 0603-00522B from the Danish Council for strategic research and the Danish Council for technology and innovation. We acknowledge financial support from the Doctoral School of Engineering and Science at Aalborg University and Otto Mønsteds Fond to Xiaoxue Tong for her visit to the University of Greenwich. We acknowledge the use of CPU times given by the EPSRC UK National Services for Computational Chemistry Software (NSCCS).

6 References

[1] M. Lotti, J. Pleiss, F. Valero, P. Ferrer, Effects of methanol on lipases: Molecular, kinetic and process issues in the production of biodiesel, Biotech. J. (2014) Epub ahead of print.

[2] F. Ma, M.A. Hanna, Biodiesel production: a review, Bioresour. Technol. 70 (1999) 1-15.

[3] P.M. Nielsen, J. Brask, L. Fjerbaek, Enzymatic biodiesel production: technical and economical considerations, Eur. J. Lipid Sci. Tech. 110 (2008) 692-700.

[4] H. Fukuda, S. Hama, S. Tamalampudi, H. Noda, Whole-cell biocatalysts for biodiesel fuel production, Trends Biotechnol. 26 (2008) 668-673.

[5] S. Cesarini, P. Diaz, P.M. Nielsen, Exploring a new, soluble lipase for FAMEs production in water-containing systems using crude soybean oil as a feedstock, Process Biochem. 48 (2013) 484-487.

[6] J.A. Price, M. Nordblad, J. Woodley, J.K. Huusom, Fed-Batch Feeding Strategies for Enzymatic Biodiesel Production, In: Proceedings of the 19th World Congress of the International Federation of Automatic Control. (2014) 6204–6209.

[7] S. Cesarini, R.F. Haller, P. Diaz, P.M. Nielsen, Combining phospholipases and a liquid lipase for one-step biodiesel production using crude oils, Biotechnol. Biofuels. 7 (2014) 29-6834-7-29.

[8] J. Price, B. Hofmann, V.T. Silva, M. Nordblad, J.M. Woodley, J.K. Huusom, Mechanistic modeling of biodiesel production using a liquid lipase formulation, Biotechnol. Prog. (2014) .

[9] U. Derewenda, L. Swenson, Y. Wei, R. Green, P.M. Kobos, R. Joerger, M.J. Haas, Z.S. Derewenda, Conformational lability of lipases observed in the absence of an oil-water interface: crystallographic studies of enzymes from the fungi *Humicola lanuginosa* and *Rhizopus delemar*, J. Lipid Res. 35 (1994) 524-534.

[10] A.M. Brzozowski, H. Savage, C.S. Verma, J.P. Turkenburg, D.M. Lawson, A. Svendsen, S. Patkar, Structural origins of the interfacial activation in *Thermomyces* (*Humicola*) *lanuginosa* lipase, Biochemistry. 39 (2000) 15071-15082.

[11] A. Svendsen, Lipase protein engineering, Biochim. Biophys. Acta. 1543 (2000) 223-238.

[12] L. Brady, A.M. Brzozowski, Z.S. Derewenda, E. Dodson, G. Dodson, S. Tolley, J.P. Turkenburg, L. Christiansen, B. Huge-Jensen, L. Norskov, *et al*. A serine protease triad forms the catalytic center of a triacylglycerol lipase, Nature. 343 (1990) 767-70.

[13] M. Kamal, P. Yedavalli, M.V. Deshmukh, N.M. Rao, Lipase in aqueous-polar organic solvents: Activity, structure, and stability, Protein Sci. 22 (2013) 904-915.

[14] C. Mattos, C.R. Bellamacina, E. Peisach, A. Pereira, D. Vitkup, G.A. Petsko, D. Ringe, Multiple solvent crystal structures: probing binding sites, plasticity and hydration, J. Mol. Biol. 357 (2006) 1471-1482.

[15] A. Tanaka, Differential scanning calorimetric studies on the thermal unfolding of *Pseudomonas cepacia* lipase in the absence and presence of alcohols, J. Biochem. 123 (1998) 289-293.

[16] C. Li, T. Tan, H. Zhang, W. Feng, Analysis of the conformational stability and activity of *Candida antarctica* lipase B in organic solvents: insight from molecular dynamics and quantum mechanics/simulations, J. Biol. Chem. 285 (2010) 28434-28441.

[17] H.J. Park, J.C. Joo, K. Park, Y.H. Kim, Y.J. Yoo, Prediction of the solvent affecting site and the computational design of stable *Candida antarctica* lipase B in a hydrophilic organic solvent, J. Biotechnol. 163 (2013) 346-352.

[18] L. Li, Y. Jiang, H. Zhang, W. Feng, B. Chen, T. Tan, Theoretical and Experimental Studies on Activity of *Yarrowia lipolytica* Lipase in Methanol/Water Mixtures, J. Phys. Chem. B. 118 (2014) 1976-1983.

[19] E.H. Kellogg, A. Leaver-Fay, D. Baker, Role of conformational sampling in computing mutation-induced changes in protein structure and stability, Proteins. 79 (2011) 830-838.

[20] Y. Liu, B. Kuhlman, RosettaDesign server for protein design, Nucleic Acids Res. 34 (2006) W235-8.

[21] R. Dennington, T. Keith, J. Millam, GaussView, version 5, *Semichem Inc*., Shawnee Mission, KS, (2009).

[22] R. Anandakrishnan, B. Aguilar, A.V. Onufriev, H++ 3.0: automating pK prediction and the preparation of biomolecular structures for atomistic molecular modeling and simulations, Nucleic Acids Res. 40 (2012) W537-41.

[23] D. Case, T. Darden, T. Cheatham III, C. Simmerling, J. Wang, R. Duke, R. Luo, R. Walker, W. Zhang, K. Merz, AMBER 12, University of California, San Francisco, (2012).

[24] J. Wang, W. Wang, P.A. Kollman, D.A. Case, Automatic atom type and bond type perception in molecular mechanical calculations, J. Mol. Graph. Model. 25 (2006) 247-260.

[25] W.L. Jorgensen, J. Chandrasekhar, J.D. Madura, R.W. Impey, M.L. Klein, Comparison of simple potential functions for simulating liquid water, J. Chem. Phys. 79 (1983) 926-935.

[26] P. Cieplak, J. Caldwell, P. Kollman, Molecular mechanical models for organic and biological systems going beyond the atom centered two body additive approximation: aqueous solution free energies of methanol and N-methyl acetamide, nucleic acid base, and amide hydrogen bonding and chloroform/water partition coefficients of the nucleic acid bases, J. Comput. Chem. 22 (2001) 1048-1057.

[27] V. Hornak, R. Abel, A. Okur, B. Strockbine, A. Roitberg, C. Simmerling, Comparison of multiple Amber force fields and development of improved protein backbone parameters, Proteins. 65 (2006) 712-725.

[28] J. Wang, R.M. Wolf, J.W. Caldwell, P.A. Kollman, D.A. Case, Development and testing of a general amber force field, J. Comput. Chem. 25 (2004) 1157-1174.

[29] A.E. Torda, R.M. Scheek, W.F. Van Gunsteren, Time-dependent distance restraints in molecular dynamics simulations, Chem. Phys. Lett. 157 (1989) 289-294.

[30] S. Miyamoto, P.A. Kollman, SETTLE: an analytical version of the SHAKE and RATTLE algorithm for rigid water models, J. Comput. Chem. 13 (1992) 952-962.

[31] D.R. Roe, T.E. Cheatham III, PTRAJ and CPPTRAJ: software for processing and analysis of molecular dynamics trajectory data, J Chem Theory Comput. 9 (2013) 3084-3095.

[32] W. Humphrey, A. Dalke, K. Schulten, VMD: visual molecular dynamics, J. Mol. Graph. 14 (1996) 33-38.

[33] M.I. Lobanov, N.S. Bogatyreva, O.V. Galzitskaia, Radius of gyration is indicator of compactness of protein structure, Mol. Biol. (Mosk). 42 (2008) 701-706.

[34] K. Zhu, A. Jutila, E.K. Tuominen, P.K. Kinnunen, Effects of i-propanol on the structural dynamics of *Thermomyces lanuginosa* lipase revealed by tryptophan fluorescence, Protein SCI. 10 (2001) 339-351.

[35] P.A. Fitzpatrick, A.C. Steinmetz, D. Ringe, A.M. Klibanov, Enzyme crystal structure in a neat organic solvent, Proc. Natl. Acad. Sci. U. S. A. 90 (1993) 8653-8657.

[36] J. Weiser, P.S. Shenkin, W.C. Still, Approximate atomic surfaces from linear combinations of pairwise overlaps (LCPO), J. Comput. Chem. 20 (1999) 217-230.

[37] K. Gekko, E. Ohmae, K. Kameyama, T. Takagi, Acetonitrile-protein interactions: amino acid solubility and preferential solvation, Biochim. Biophys. Acta. 1387 (1998) 195-205.

[38] P. Sashi, U.M. Yasin, A.K. Bhuyan, Unfolding action of alcohols on a highly negatively charged state of cytochrome c, Biochemistry. 51 (2012) 3273-3283.

[39] H.J. Park, K. Park, Y.J. Yoo, Understanding the effect of tert-butanol on *Candida antarctica* lipase B using molecular dynamics simulations, Mol. Simulat. 39 (2013) 653-659.

[40] L. Yang, J.S. Dordick, S. Garde, Hydration of enzyme in nonaqueous media is consistent with solvent dependence of its activity, Biophys. J. 87 (2004) 812-821.

[41] P. Hünenberger, A. Mark, W. Van Gunsteren, Fluctuation and cross-correlation analysis of protein motions observed in nanosecond molecular dynamics simulations, J. Mol. Biol. 252 (1995) 492-503.

[42] A. Dror, E. Shemesh, N. Dayan, A. Fishman, Protein engineering by random mutagenesis and structure-guided consensus of *Geobacillus stearothermophilus* Lipase T6 for enhanced stability in methanol, Appl. Environ. Microbiol. 80 (2014) 1515-1527.

[43] M.T. Reetz, P. Soni, L. Fernández, Y. Gumulya, J.D. Carballeira, Increasing the stability of an enzyme toward hostile organic solvents by directed evolution based on iterative saturation mutagenesis using the B-FIT method, Chem. Commun (Camb). 46 (2010) 8657-8658.

[44] A. Zaks, A.M. Klibanov, The effect of water on enzyme action in organic media, J. Biol. Chem. 263 (1988) 8017-8021.

[45] L.A.S. Gorman, J.S. Dordick, Organic solvents strip water off enzymes, Biotechnol. Bioeng. 39 (1992) 392-397.

[46] R. Wedberg, J. Abildskov, G.H. Peters, Protein dynamics in organic media at varying water activity studied by molecular dynamics simulation, J. Phys. Chem. B. 116 (2012) 2575-2585.

[47] A. Cruz, E. Ramirez, A. Santana, G. Barletta, G.E. López, Molecular dynamic study of subtilisin Carlsberg in aqueous and nonaqueous solvents, Mol. Simulat. 35 (2009) 205-212.

[48] P.P. Wangikar, P.C. Michels, D.S. Clark, J.S. Dordick, Structure and function of subtilisin BPN' solubilized in organic solvents, J. Am. Chem. Soc. 119 (1997) 70-76.

[49] N.M. Micaêlo, C.M. Soares, Modeling hydration mechanisms of enzymes in nonpolar and polar organic solvents, FEBS J. 274 (2007) 2424-2436.

[50] A. Badoei-Dalfard, K. Khajeh, S.M. Asghari, B. Ranjbar, H.R. Karbalaei-Heidari, Enhanced activity and stability in the presence of organic solvents by increased active site polarity and stabilization of a surface loop in a metalloprotease, J. Biochem. 148 (2010) 231-238.

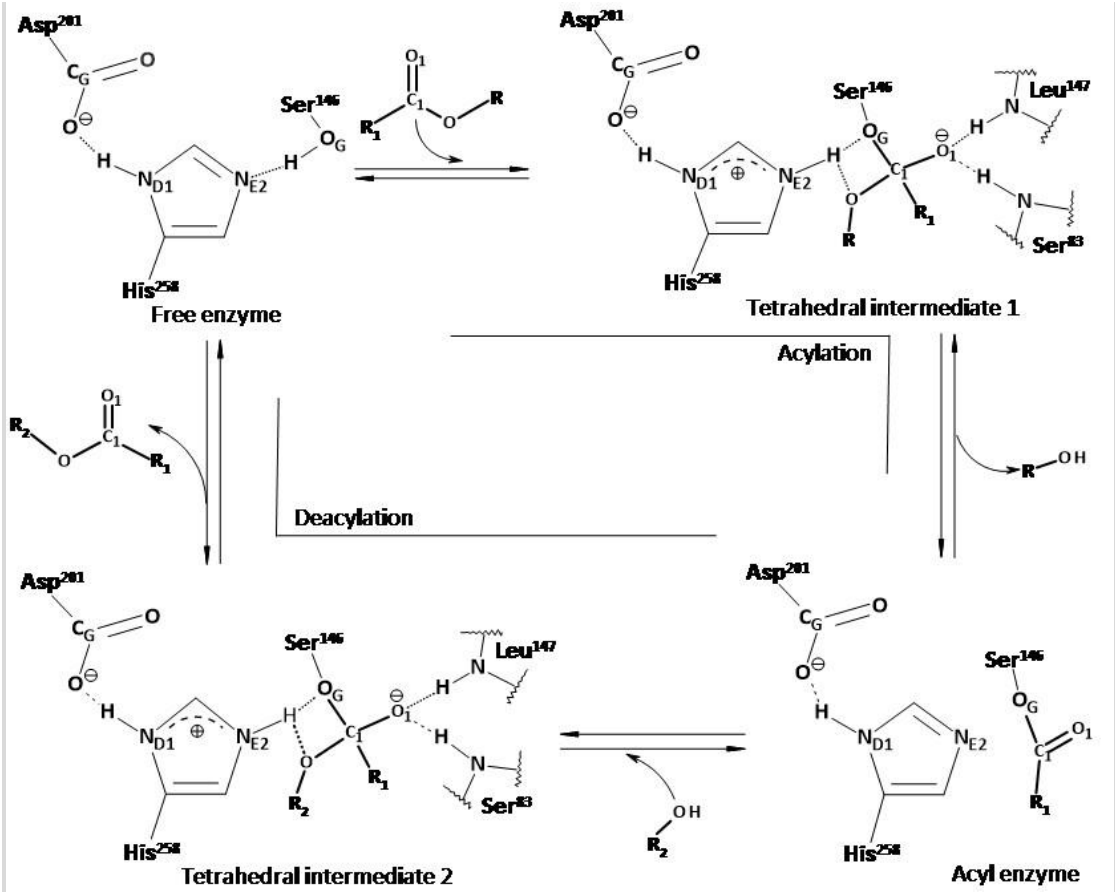

Fig. 1. Catalytic mechanism of *Thermomyces lanuginosus* lipase for methanolysis or hydrolysis reaction. R_1COOR represents the fatty acid ester substrate. R_2OH represents the methanol molecule in methanolysis reaction or the water molecule in hydrolysis reaction. CG: carbon atom in the side-chain carboxyl group of Asp^{201}. ND1 and NE2: nitrogen atoms from His^{258} ring. OG: Ser^{146} hydroxyl oxygen atom. O1: carbonyl oxygen of the ester. C1: carbonyl carbon of the ester.

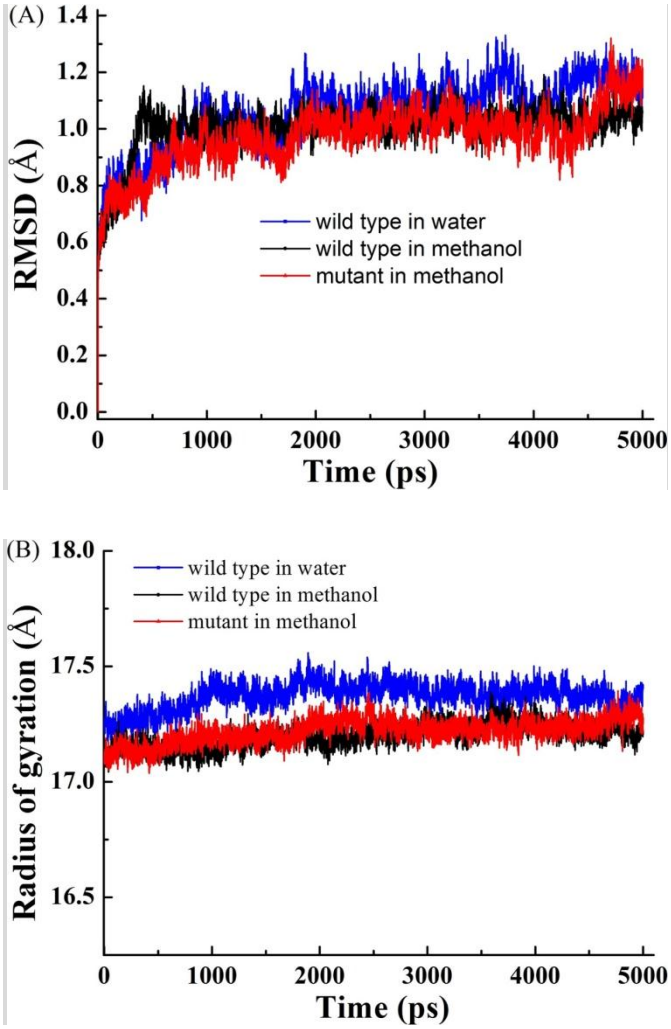

Fig. 2. RMSDs of the backbone heavy atoms (A) and radius of gyration (B) as a function of the simulation time for both the WT TLL and the TLL I241E mutant. Blue solid lines, the WT in water; Black solid lines, the WT in methanol; Red solid lines, the mutant in methanol.

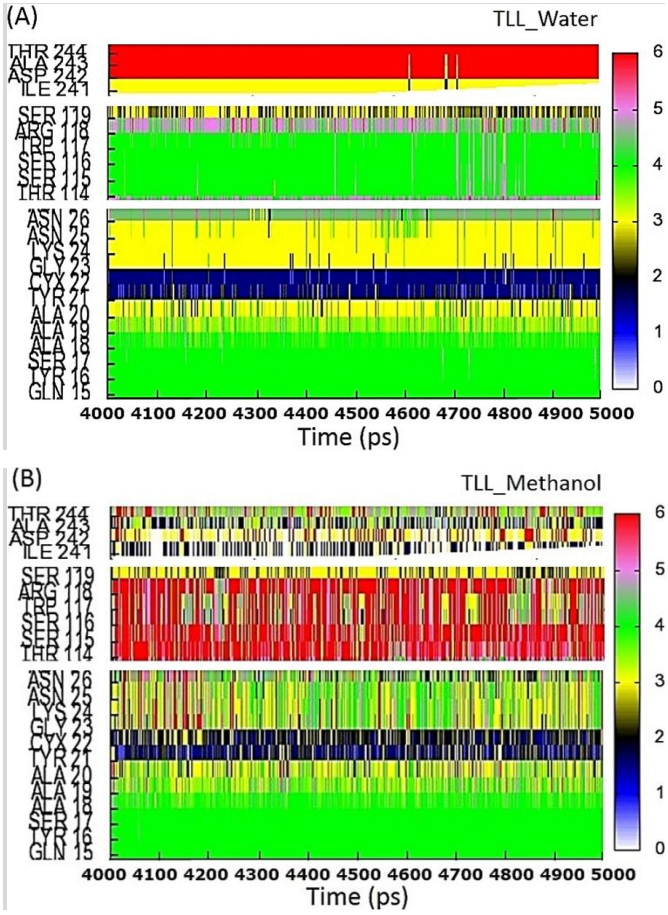

Fig. 3. Secondary structural types of WT TLL residues 23-26, 114-119 and 241-244 in water (A) and in methanol (B) as a function of the simulation time. Each residue (y-axis) is assigned a secondary structural type (0 = no structure, 1 = parallel β strand, 2 = antiparallel β strand, 3 = 3_{10}-helix, 4 = α-helix, 5 = Pi helix, 6 = turn). The same color code is adopted in all plots (0, white; 1, blue; 2, black; 3, yellow; 4, green; 5, violet; and 6, red).

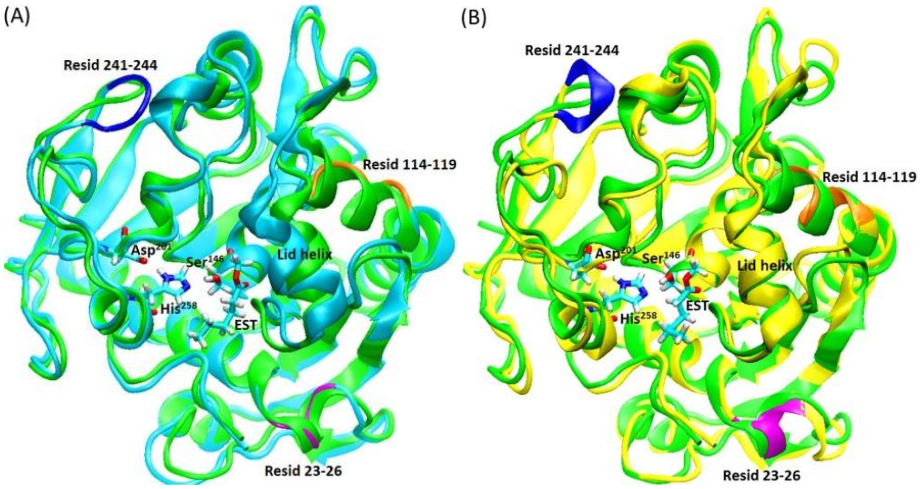

Fig. 4. Superimposition of the last structures from MD simulations of WT TLL in water (cyan color in figure A) and in methanol (yellow color in figure B) with the reference crystallographic structure (green color). Residues 23-26 are colored in magenta, residues 114-119 in orange, and residues 241-244 in blue. Lid helix (residues 86-92) are marked. Catalytic triad residues (Ser^{146}-Asp^{201}-His^{258}) and ester substrate (EST) are labelled and represented in bonds.

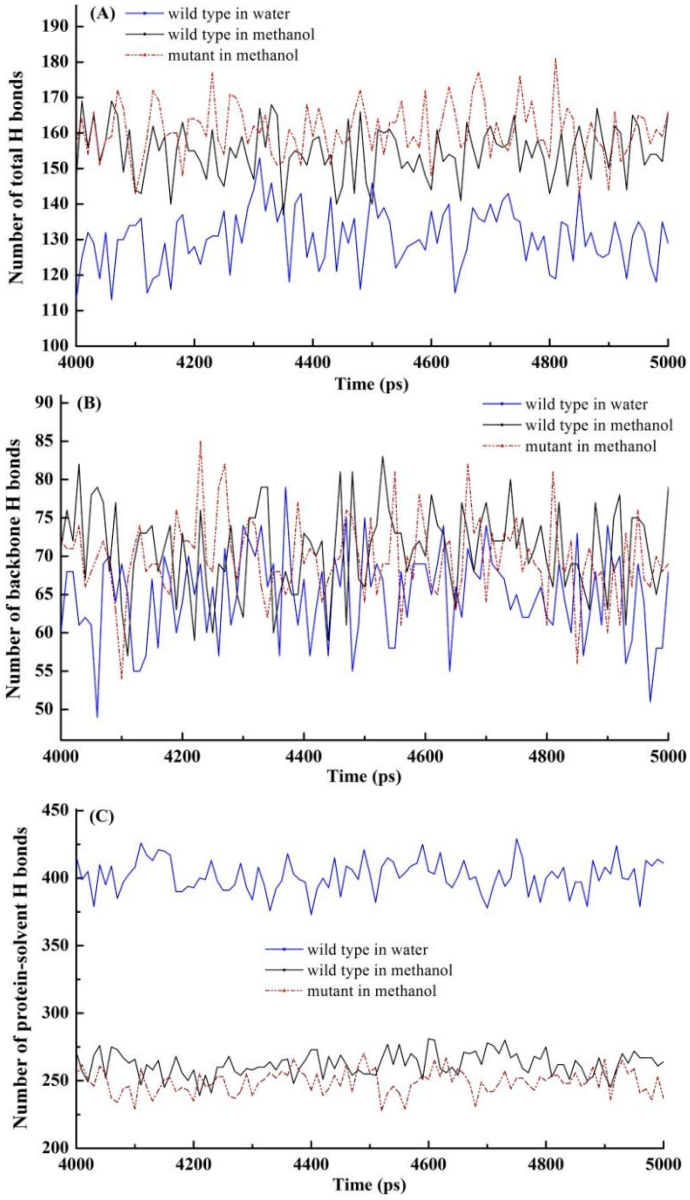

Fig. 5. The number of H-bonds present in the WT and the mutant over the course of the simulations. (A) the number of total protein-protein H-bonds; (B) the number of intra-protein backbone H-bonds; (C) the number of protein-solvent H-bonds. Blue solid lines, the WT in water; Black solid lines, the WT in methanol; Red dash lines, the mutant in methanol.

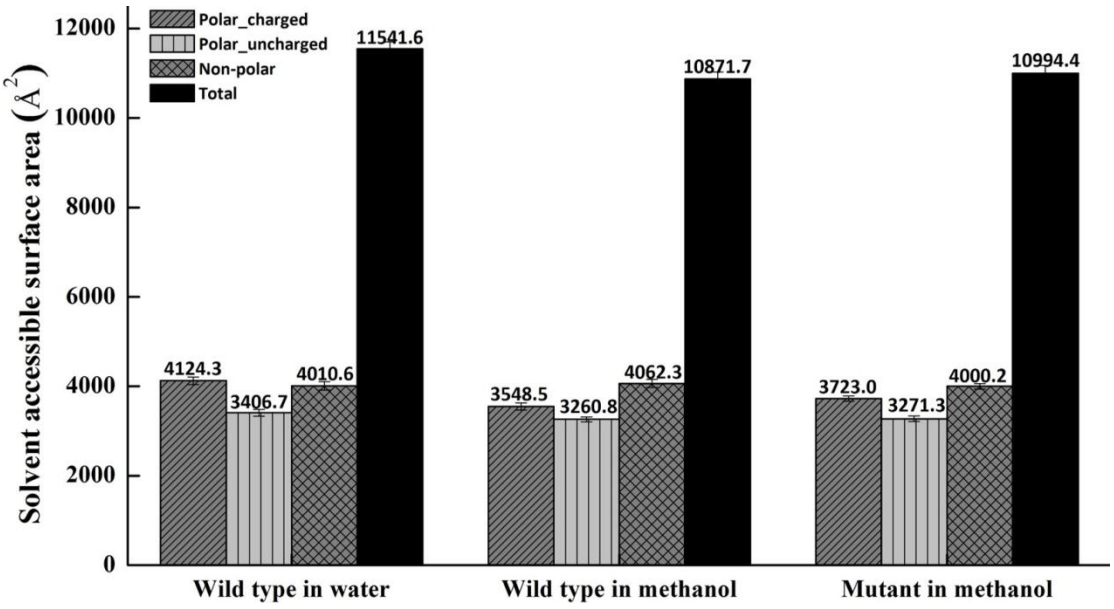

Fig. 6. Solvent accessibility of amino acid residues for the WT in two solvents and the mutant in methanol. Non-polar amino acids are amino acids Ala, Ile, Leu, Phe, Val, Pro and Gly. Polar uncharged amino acids are amino acids Gln, Asn, Ser, Thr, Tyr and Trp. Polar charged amino acids are amino acids Arg, Lys, Asp, Glu and His with hydrogens on both nitrogens.

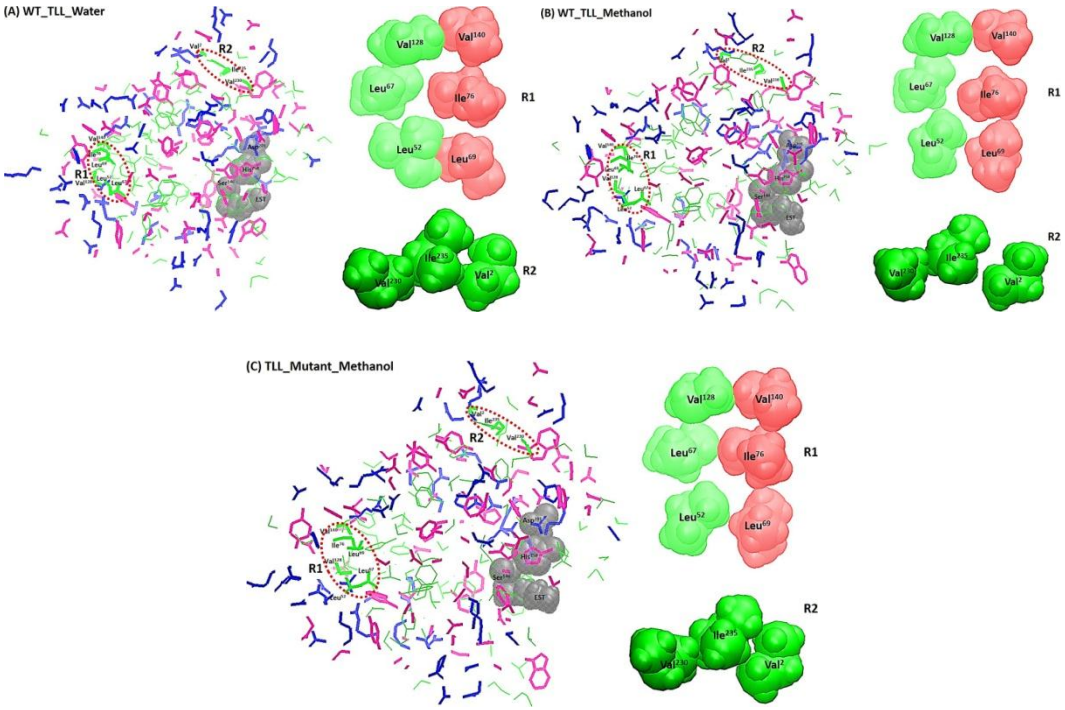

Fig. 7. Distribution of non-polar and polar amino acid residues in the structures from the last snapshot of three simulation trajectories (left) and the van der Waals packing between the core residues in two hydrophobic regions of R1 and R2 (right). (A) The WT in water. (B) The WT in methanol. (C) The mutant in methanol. The same color code is adopted in all plots (hydrophobic amino acids, green; polar uncharged amino acids, magenta; and charged amino acids, blue). The backbones are superimposed before the structural comparison. Only the side chains of amino acid residues are shown. The core residues in R1 (Leu^{52}, Leu^{69}, Leu^{67}, Ile^{76}, Val^{128} and Val^{140}) and R2 (Val^{2}, Val^{230} and Ile^{235}) are labelled and displayed in bold green lines. Catalytic triad residues and EST substrate are also displayed (light grey).

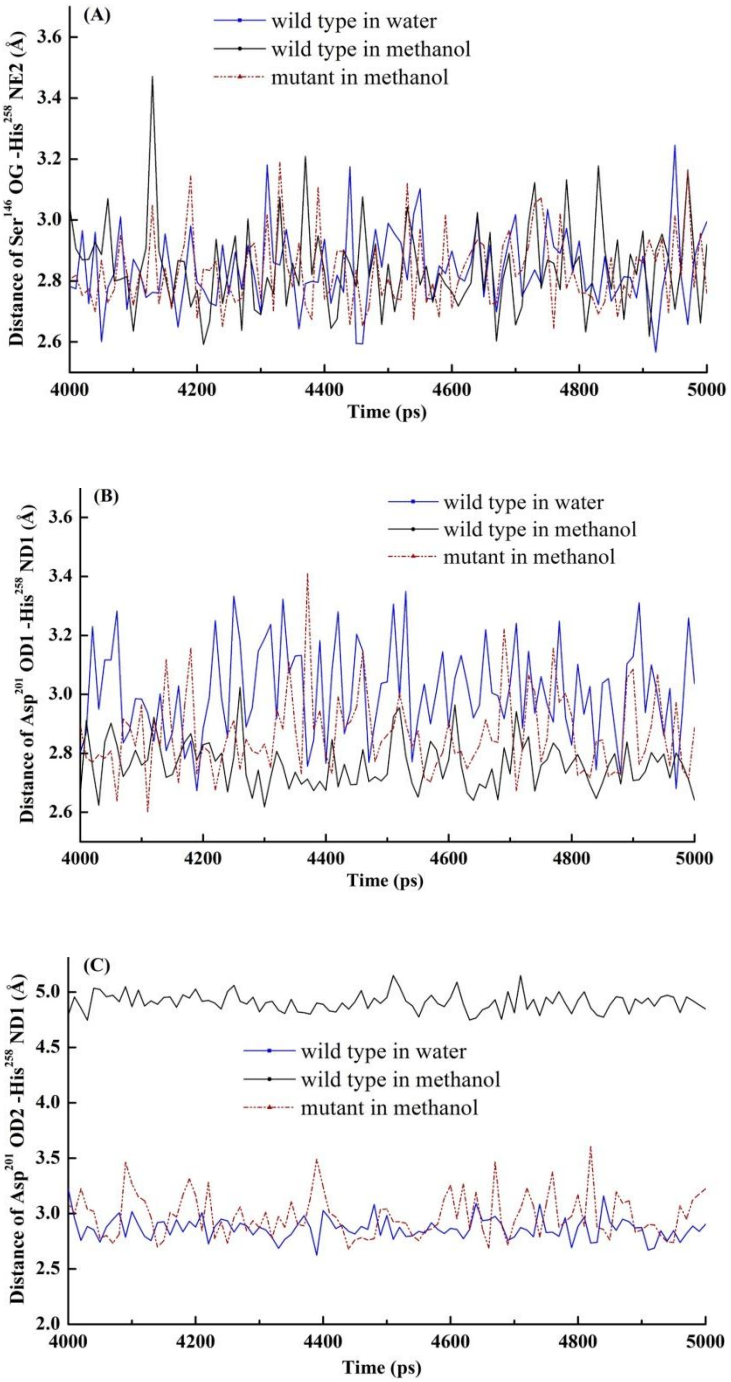

Fig.8. H-bond distance between the catalytic triad residues for the WT in two solvents and the mutant in methanol along the simulations. (A) Distance between Ser^{146} OG and His^{258} NE2. (B) Distance between Asp^{201} OD1 and His^{258} ND1. (C) Distance between Asp^{201} OD2 and His^{258} ND1. OD1 and OD2: oxygen atoms from Asp^{201} side chain. ND1 and NE2: nitrogen atoms from His^{258} ring. OG: Ser^{146} hydroxyl oxygen atom. Blue solid lines, the WT in water; Black solid lines, the WT in methanol; Red dash lines, the mutant in methanol.

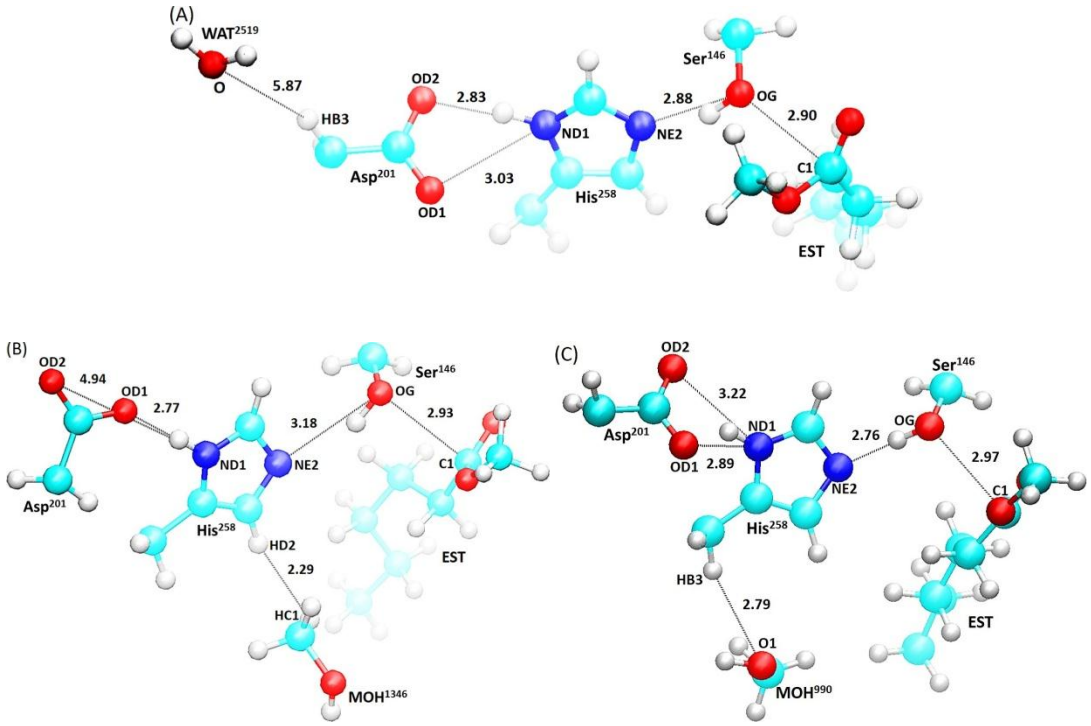

Fig.9. Hydrogen-bonding interactions among the catalytic triad residues and the closest solvent molecule around the triad. (A) The WT in water (WAT). (B) The WT in methanol (MOH). (C) The mutant in methanol (MOH). Only the side chain of each amino acid residue (Ser^{146}, Asp^{201} and His^{258}) is shown. Amino acid residues and ester substrate (EST) are shown in CPK model. OD1 and OD2: oxygen atoms from Asp^{201} side chain. ND1 and NE2: nitrogen atoms from His^{258} ring. OG: Ser^{146} hydroxyl oxygen atom. Carbon atoms are colored in cyan, nitrogen atoms in blue, oxygen atoms in red, hydrogen atoms in white.

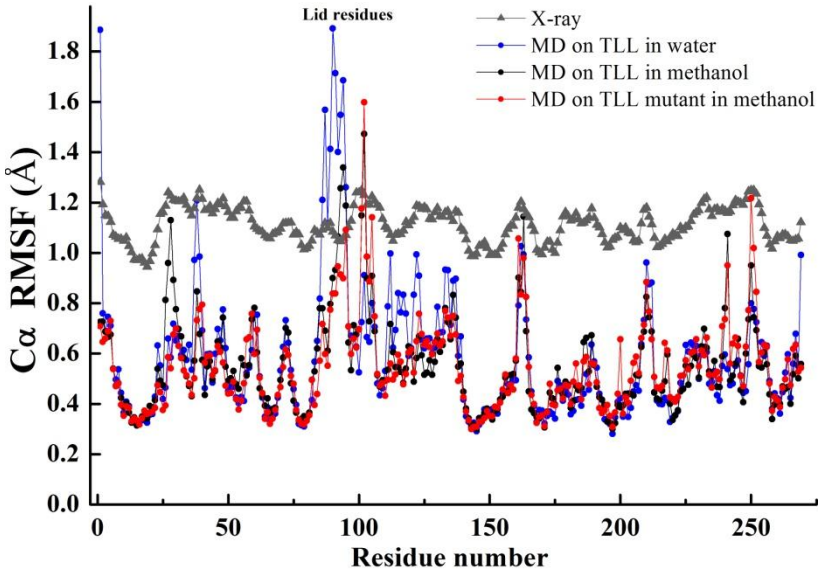

Fig. 10. Cα RMSFs from the MD simulations and the X-ray structure. The Cα RMSF of the crystal structure is calculated from the X-ray Cα B-factor data with the standard equation RMSF = $(3B/8\pi^2)^{1/2}$ where B = B-factor of the Cα atom.